

Periodic lump, soliton, and some mixed solutions of the (2+1)-dimensional generalized coupled nonlinear Schrödinger equations

Xiao-Min Wang(王晓敏), Ji Li(李吉), and Xiao-Xiao Hu(胡霄骁)
Citation: Chin. Phys. B, 2025, 34 (**11**): 110502. DOI: 10.1088/1674-1056/ae1019
http://cpb.iphy.ac.cn; http://iopscience.iop.org/cpb

What follows is a list of articles you may be interested in

Different wave patterns for two-coupled Maccari's system with complex structure via truncated Painlevé approach

Hongcai Ma(马红彩), Xinru Qi(戚心茹), and Aiping Deng(邓爱平)
Chin. Phys. B, 2023, 32 (**12**): 120503. DOI: 10.1088/1674-1056/acf497

Analytical three-periodic solutions of Korteweg-de Vries-type equations

Mi Chen(陈觅) and Zhen Wang(王振)
Chin. Phys. B, 2023, 32 (**9**): 090504. DOI: 10.1088/1674-1056/acd9c4

General *M*-lumps, *T*-breathers, and hybrid solutions to (2+1)-dimensional generalized KDKK equation

Peisen Yuan(袁培森), Jiaxin Qi(齐家馨), Ziliang Li(李子良), and Hongli An(安红利)
Chin. Phys. B, 2021, 30 (**4**): 040503. DOI: 10.1088/1674-1056/abcf9f

Localized characteristics of lump and interaction solutions to two extended Jimbo-Miwa equations

Yu-Hang Yin(尹宇航), Si-Jia Chen(陈思佳), and Xing Lü(吕兴)
Chin. Phys. B, 2020, 29 (**12**): 120502. DOI: 10.1088/1674-1056/aba9c4

Lump, lumpoff and predictable rogue wave solutions to a dimensionally reduced Hirota bilinear equation

Haifeng Wang(王海峰), Yufeng Zhang(张玉峰)
Chin. Phys. B, 2020, 29 (**4**): 040501. DOI: 10.1088/1674-1056/ab75d7

Periodic lump, soliton, and some mixed solutions of the (2+1)-dimensional generalized coupled nonlinear Schrödinger equations

Xiao-Min Wang(王晓敏)[1,2,†], Ji Li(李吉)[1,2], and Xiao-Xiao Hu(胡霄骁)[3]

[1] *Department of Physics, Taiyuan Normal University, Jinzhong* 030619, *China*
[2] *Institute of Computational and Applied Physics, Taiyuan Normal University, Jinzhong* 030619, *China*
[3] *Shanxi Chinese Medicine School, Shanxi Health Vocational University, Taiyuan* 030012, *China*

(Received 15 July 2025; revised manuscript received 29 September 2025; accepted manuscript online 7 October 2025)

The (2+1)-dimensional generalized coupled nonlinear Schrödinger equations with a four-wave mixing term are studied in this paper, which describe optical solitons in birefringent fibers. Utilizing the Hirota bilinear method, we systematically construct single- and double-periodic lump solutions. To provide a detailed insight into the dynamic behavior of the nonlinear waves, we explore diverse mixed solutions, including bright-dark, W-shaped, multi-peak, and bright soliton solutions. Building upon single-periodic lump solutions, we analyze the dynamics of lump waves on both plane-wave and periodic backgrounds using the long-wave limit method. Moreover, we obtain the interaction solutions involving lumps, periodic lumps, and solitons. The interactions among two solitons, multiple lumps, and mixed waves are illustrated and analyzed. Comparative analysis reveals that these multi-lump solutions exhibit richer dynamical properties than conventional single-lump ones. These results contribute to a deeper understanding of nonlinear systems and may facilitate solving nonlinear problems in nature.

Keywords: nonlinear Schrödinger equations, lump solutions, mixed solutions, Hirota bilinear method

PACS: 05.45.Yv, 02.70.Wz, 87.10.Ed

DOI: 10.1088/1674-1056/ae1019 **CSTR:** 32038.14.CPB.ae1019

1. Introduction

The coupled nonlinear Schrödinger (NLS) equations have long served as cornerstone models for understanding wave dynamics in diverse physical systems, including nonlinear optics, Bose–Einstein condensates, and plasma physics.[1–6] These equations describe the evolution of wave envelopes in dispersive media, where a balance between nonlinearity and dispersion sustains localized structures such as solitons.[7–9] The study of coupled NLS systems has seen significant advancements in modeling multi-component wave interactions, particularly in polarization-resolved light propagation in birefringent fibers[10] and spinor condensate dynamics in ultracold quantum gases[11] in recent decades. The generalized coupled NLS equations provide a versatile platform for discovering non-classical coherent structures beyond conventional solitons, which incorporate cross-phase modulation (XPM), four-wave mixing (FWM), and higher-order nonlinear terms. Moreover, previous studies have shown that FWM exerts the strongest influence on optical systems.[12] The localized wave solutions of the generalized coupled NLS equations include lumps, breathers, and rogue waves, each demonstrating distinct dynamical characteristics. Breathers exhibit periodic oscillatory behavior along specific propagation directions,[13] with lump waves emerging as infinite-period limits of breathers. Characterized by spatial localization and algebraic decay properties, lump solutions were originally discovered in the context of the KP-I equation,[14] and their two-dimensional energy-localized profiles have proven instrumental for modeling shallow-water wave interactions and magnetized plasma phenomena.

Recent theoretical developments have expanded lump-wave analysis within NLS systems through a modified Hirota bilinear method, enabling exact multi-lump constructions; numerical simulations have demonstrated breather-like amplitude oscillations[15,16] in (2+1)-dimensional NLS systems and energy oscillation patterns[17] in multicomponent lump interactions. Notably, lumps on periodic backgrounds have been linked to extreme wave events.[18,19] Moreover, the rogue wave and the lump wave can be transformed into the W-shaped soliton, and the breather can be converted into several kinds of nonlinear waves under specific conditions. These findings establish unified frameworks for understanding nonlinear wave metamorphosis across hydrodynamics and nonlinear optical systems.[20–23] The interplay between solitons and lump waves introduces novel paradigms for energy transfer and waveform engineering across nonlinear systems.[24–28] In single-component systems, solitons and lumps establish bound states through nonlinear resonance mechanisms, with stability governed by phase synchronization and velocity alignment.[29,30]

†Corresponding author. E-mail: wangxiaomin086@163.com

© 2025 Chinese Physical Society and IOP Publishing Ltd. All rights, including for text and data mining, AI training, and similar technologies, are reserved.

In particular, the superposition mechanisms, state transitions, and internal connections among various nonlinear waves have been extensively studied.[31,32] In generalized coupled NLS systems, cross-component nonlinear coupling enables richer interaction scenarios, for instance, solitons acting as nonlinear catalysts to induce lump fission via parametric amplification, or lump chains modulating soliton trajectories through XPM.[33] A generalized coupled NLS system with an FWM effect to describe optical solitons in a birefringent fiber is proposed[34]

$$\mathrm{i}u_{jt}+u_{jxx}+u_{jyy}+2(a|u_1|^2+c|u_2|^2+bu_1\bar{u}_2+\bar{b}\bar{u}_1u_2)u_j=0,\quad j=1,2, \tag{1}$$

where u_j, depending on x, y, and t, describes the envelopes of the two circularly polarized waves. The variables t and x represent the delay time and normalized distance, respectively; a and c are real constants accounting for self-phase modulation and XPM; b is a complex constant representing the FWM effect, and $\bar{b}$, $\bar{u}_1$, and $\bar{u}_2$ are the complex conjugates of b, u_1, and u_2. Although extensive research has been conducted on one-dimensional systems, several issues remain to be explored.[35–40] Bright soliton solutions for Eq. (1) have been studied in Ref. [34]. However, lump solutions and the mixed solutions of lumps and solitons have not been discussed for Eq. (1). In this paper, we will obtain multiple nonlinear wave solutions, including periodic lumps, multi-lumps, and mixed solutions of lumps and solitons, by the Hirota bilinear approach and the long-wave limit method. Considering that nonlinear wave solutions of high-dimensional equations are structurally more complex, they may exhibit richer physical phenomena.[41–43]

The structure of this paper is organized as follows. In Section 2, we will obtain single- and double-periodic lump solutions for Eq. (1) by the Hirota bilinear method. In Section 3, we will display lump solutions and mixed solutions of lumps, periodic lumps, and solitons by applying the long-wave limit method to the periodic lump and soliton solutions. Finally, the conclusions are summarized in Section 4.

2. Periodic lump solutions of the coupled NLS equations

In Refs. [44–46], single-periodic lump solutions for certain nonlinear evolution equations have been constructed by introducing a combination function of hyperbolic cosine and trigonometric cosine. In this part, we acquire the bilinear form and the mixed single- and double-periodic lump solutions of Eq. (1) via the Hirota method. To begin with, we introduce the dependent variable transformations $u_j=G_j/F$, where G_j are complex functions and F is a real one. Substituting the above transformations into Eq. (1), we obtain its bilinear form as follows:

$$\mathrm{i}D_tG_j\cdot F+D_x^2G_j\cdot F+D_y^2G_j\cdot F-\lambda G_j\cdot F=0, \tag{2}$$

$$2a|G_1|^2+2c|G_2|^2+2bG_1G_2^*+2b^*G_1^*G_2 -D_x^2F\cdot F-D_y^2F\cdot F+\lambda F\cdot F=0, \tag{3}$$

where D denotes the Hirota bilinear operator, defined as

$$D_v^pD_\zeta^qa\cdot b=\left(\frac{\partial}{\partial v}-\frac{\partial}{\partial v'}\right)^p\left(\frac{\partial}{\partial\zeta}-\frac{\partial}{\partial\zeta'}\right)^q \times a(v,\zeta)b(v',\zeta')|_{v'=v,\zeta'=\zeta},$$

where p and q are both positive integers, a is a function of v and ζ, and b is a function of v' and ζ'.

2.1. Single periodic lump solution

To derive the single-periodic lump solution of Eq. (1), G_j and F are expanded as $F=1+\varepsilon^2f_2(x,y,t)$ and

$$G_j=m_jg_0(x,y,t)+n_j\varepsilon g_1(x,y,t) +\varepsilon^2m_jg_0(x,y,t)g_2(x,y,t), \tag{4}$$

where ε is a formal expansion parameter. Substituting the expanded forms of G and F into the bilinear Eqs. (2) and (3), and taking $\varepsilon=1$ without loss of generality, the single-periodic solution of Eq. (1) is obtained as follows:

$$u_j=\frac{\delta_1m_j\gamma_0+\Theta_1n_j\alpha_1+\delta_1m_j\gamma_0Z_1\rho\Theta_{11}}{1+\rho\Theta_{11}}, \tag{5}$$

where we assume

$$\delta_1=\cos\xi_0+\mathrm{i}\sin\xi_0,\quad \Theta_1=\cosh\theta_1+\sinh\theta_1,\quad \Theta_{11}=\cosh\theta_{11}+\sinh\theta_{11}, \tag{6}$$

and $\theta_1=k_{11}x+k_{21}y+\mathrm{i}(-\lambda+k_{11}^2+k_{21}^2)t+\xi_1$, $\theta_{11}=\theta_1+\overline{\theta}_1$, $\xi_0=k_{10}x+k_{20}y-(\lambda+k_{10}^2+k_{20}^2)t$, and $\rho=\mathrm{e}^\zeta$. The parameters satisfy the constraint conditions

$$\lambda=2(a|m_1|^2+\bar{b}m_2\overline{m}_1+bm_1\overline{m}_2+c|m_2|^2)|\gamma_0|^2,$$

$$m_1=\frac{-\bar{b}m_2\bar{n}_1-cm_2\bar{n}_2}{a\bar{n}_1+b\bar{n}_2},\quad Z_1=\frac{(k_{10}+\mathrm{i}k_{11})c_{11}+(k_{20}+\mathrm{i}k_{21})c_{22}}{(k_{10}-\mathrm{i}\bar{k}_{11})c_{11}+(k_{20}-\mathrm{i}\bar{k}_{21})c_{22}},$$

$$\mathrm{e}^\zeta=\frac{2l|\alpha_1|^2}{2c_{11}^2+2c_{22}^2-\lambda(Z_1+\overline{Z}_1-2)}, \tag{7}$$

$$l=a|n_1|^2+\bar{b}n_2\bar{n}_1+bn_1\bar{n}_2+c|n_2|^2. \tag{8}$$

In the above expressions, k_{10} and k_{20} are arbitrary real constants, γ_0, k_{11}, k_{21}, m_j, n_j, and α_1 are arbitrary complex constants, $c_{11}=k_{11}+\bar{k}_{11}$, and $c_{22}=k_{21}+\bar{k}_{21}$. Since u_j $(j=1,2)$ have similar properties, we only consider the

results obtained for u_1. Figure 1 shows the motion process of the single-periodic lump wave, whose speed and waveform remain unchanged. Compared with Fig. 1, when the imaginary part of k_{11} increases while other parameter values remain constant, the period of the periodic lump decreases. When $t=0$, Fig. 2(a) shows the three- dimensional plot, and the corresponding contour map of the periodic lump solution in the (x,y) plane is shown in Fig. 2(b).

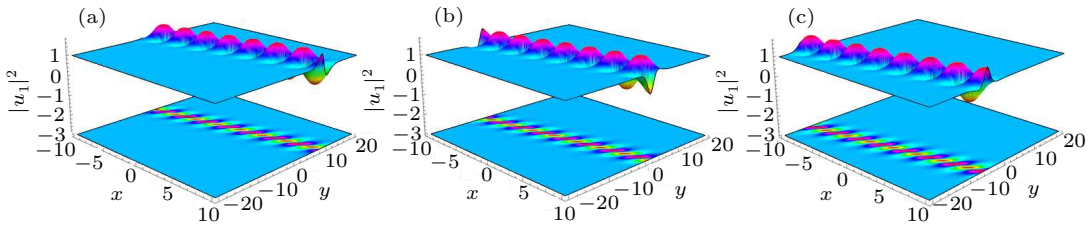


Fig. 1. Motion of a single periodic lump for Eq. (1) via solution (5) with parameters $a=1$, $b=1$, $c=1$, $k_{11}=0.4+3.5\mathrm{i}$, $k_{21}=-1+0.5\mathrm{i}$, $k_{10}=1$, $k_{20}=1$, $m_2=0.5$, $n_1=1$, $n_2=1$, $\alpha_1=1$, $\gamma_0=2$, $\xi_1=0$; (a) $t=-4$, (b) $t=0$, (c) $t=4$.

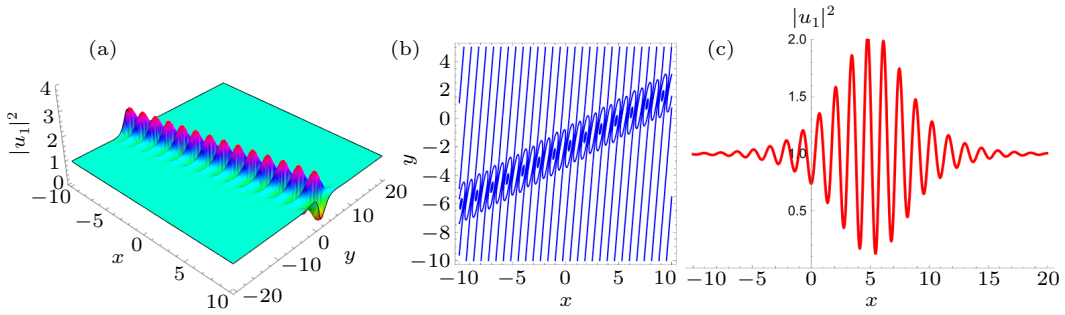


Fig. 2. Plots of a single periodic lump for Eq. (1) via solution (5) with $k_{11}=0.4+5.5\mathrm{i}$; (a) three-dimensional plot; (b) contour profile; (c) cross-sectional view of (a).

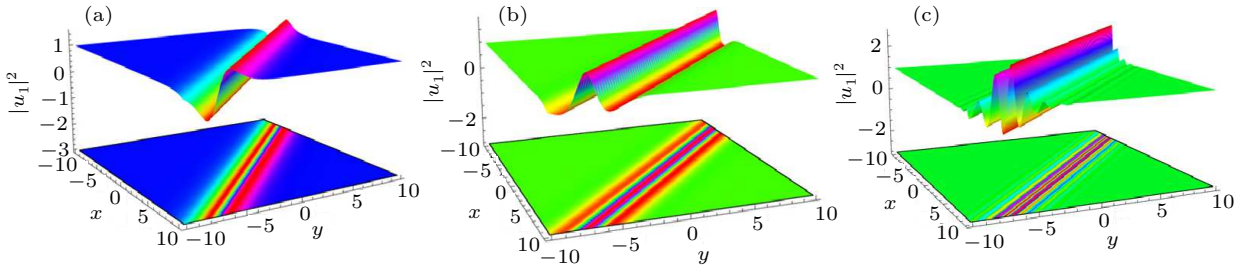


Fig. 3. Transformation of one periodic lump of Eq. (1) with the following parameters: (a) $k_{11}=k_{21}=1+0.1\mathrm{i}$; (b) $k_{11}=k_{21}=1+0.9\mathrm{i}$; (c) $k_{11}=k_{21}=1+5\mathrm{i}$.

If appropriate parameters are chosen, a single periodic lump can transform into bright–dark, W-shaped, and multi-peak solitons. To investigate the conversion mechanism of the periodic lump solution, Eq. (5) can be rewritten as follows:

$$u_j = \mathrm{e}^{\mathrm{i}\xi_0}\left[\frac{m_j}{2}\gamma_0(1+Z_1)-\frac{m_j}{2}\gamma_0(1-Z_1)\frac{\sinh(\Lambda_1)}{\cosh(\Lambda_1)} + \frac{n_j\alpha_1}{2\mathrm{e}^{\frac{\xi}{2}}}\frac{\cos(\Lambda_2)+\mathrm{i}\sin(\Lambda_2)}{\cosh(\Lambda_1)}\right], \tag{9}$$

where

$$\begin{aligned}\Lambda_1 &= k_{11R}x+k_{21R}y-2(k_{11R}k_{11I}+k_{21R}k_{21I})t+\xi_1+\frac{\zeta}{2},\\ \Lambda_2 &= -(k_{11I}+k_{10})x-(k_{21I}+k_{20})y\\ &\quad+(k_{11I}^2-k_{11R}^2+k_{21I}^2-k_{21R}^2+k_{10}^2+k_{20}^2+2\lambda)t,\end{aligned} \tag{10}$$

and the subscripts R and I denote the real and imaginary parts, respectively. Other parameters are defined as before.

From Eq. (9), it can be clearly seen that the periodic lump solution involves both hyperbolic and trigonometric functions, which jointly determine its essential characteristics. The hyperbolic functions (cosh, sinh) govern the localization of the wave, while the trigonometric functions (cos, sin) define its periodicity. The single periodic lump possesses two characteristic lines, $\Lambda_1=0$ and $\Lambda_2=0$, which dictate its dynamical behavior. When the following condition is satisfied

$$\begin{vmatrix} k_{11R} & k_{21R} \\ k_{11I}+k_{10} & k_{21I}+k_{20}\end{vmatrix}=0,$$

the two characteristic lines become parallel, leading to the transformation of the single periodic lump into various types of nonlinear waves.

To explore this transformation, we vary the ratio $(k_{11I}+k_{10})/k_{11R}$ while fixing the parameters as $a=b=c=1$, $k_{10}=k_{20}=\xi_1=0$, $m_2=n_1=n_2=1$, $\alpha_1=\gamma_0=0.1$, $t=0$,

and $k_{11R} = 1$. When $|k_{11I}| \leq 0.5$, the solution (9) represents a bright–dark soliton, as illustrated in Fig. 3(a). For $0.5 < |k_{11I}| < 1.4$, the solution exhibits a W-shaped soliton with a single peak and two valleys, as shown in Fig. 3(b). As $|k_{11I}|$ further increases ($|k_{11I}| \geq 1.4$), the oscillations become sharper, and the periodic lump evolves into an asymmetric multi-peak soliton, as displayed in Fig. 3(c).

In addition, by setting $\gamma_0 = 0$, Eq. (9) reduces to a bright one-soliton solution, as shown in Fig. 4.

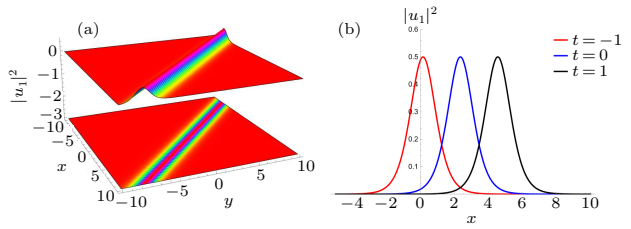


Fig. 4. Bright one-soliton solutions for Eq. (1). (a) Three-dimensional plot and (b) two-dimensional plot of the soliton, with parameters chosen as in Fig. 1 except $k_{11} = 1+0.1\mathrm{i}$, $k_{21} = 1+\mathrm{i}$, $m_2 = 1$, and $\gamma_0 = 0$.

Investigation of the linear stability of the solutions to the NLS equations is regarded as one of the most important aspects of nonlinear wave theory. In the following, taking the single periodic lump solution as an example, we analyze its linear stability. For simplicity, we denote

$$u_j = u_{0j}\,\mathrm{e}^{\mathrm{i}(\sigma x+\rho y+rt)}. \tag{11}$$

Substituting Eq. (11) into Eq. (1), we obtain

$$r = 2au_{01}^2 + 2bu_{01}u_{02} + 2\bar{b}u_{01}u_{02} + 2cu_{02}^2 - \rho^2 - \sigma^2, \tag{12}$$

where u_{0j}, σ, and ρ are all real constants. Next, we add a disturbance term to Eq. (11), and the constant solutions u_j can be expressed as

$$u_j = \left(u_{0j} + \vartheta v_j\right)\mathrm{e}^{\mathrm{i}(\sigma x+\rho y+rt)}, \tag{13}$$

where ϑ is a disturbance parameter, and v_j is defined as

$$v_j = \Lambda_{1j}\,\mathrm{e}^{\mathrm{i}(\sigma_0 x+\rho_0 y-r_0 t)} + \Lambda_{2j}\,\mathrm{e}^{-\mathrm{i}(\sigma_0 x+\rho_0 y-r_0 t)}. \tag{14}$$

Here, Λ_{1j} and Λ_{2j} are coefficients of the linear combination, while σ_0, ρ_0, and r_0 denote the real disturbance wave numbers and the real disturbance frequency, respectively. Substituting Eq. (13) into Eq. (1), we have

$$\begin{aligned}&\mathrm{i}v_{jt} + 2\mathrm{i}\rho v_{jy} + v_{jyy} + 2\mathrm{i}\sigma v_{jx} + v_{jxx} + M_1u_{0j}v_1\\ &+M_2u_{0j}\bar{v}_1 + M_3u_{0j}v_2 + M_4u_{0j}\bar{v}_2 = 0,\end{aligned} \tag{15}$$

where $\bar{v}_j$ denotes the complex conjugate of v_j, and

$$\begin{aligned}&M_1 = 2au_{01} + 2bu_{02},\ \ M_2 = 2au_{01} + 2\bar{b}u_{02},\\ &M_3 = 2\bar{b}u_{01} + 2cu_{02},\ \ M_4 = 2bu_{01} + 2cu_{02}.\end{aligned} \tag{16}$$

Then, substituting Eq. (14) into Eq. (15) and linearizing the equations with respect to Λ_{1j} and Λ_{2j}, we derive

$$\begin{aligned}&\psi_{11}\Lambda_{11} + M_2u_{01}\Lambda_{21} + M_3u_{01}\Lambda_{12} + M_4u_{01}\Lambda_{22} = 0,\\ &M_2u_{01}\Lambda_{11} + \psi_{22}\Lambda_{21} + M_4u_{01}\Lambda_{12} + M_3u_{01}\Lambda_{22} = 0,\\ &M_1u_{02}\Lambda_{11} + M_2u_{02}\Lambda_{21} + \psi_{33}\Lambda_{12} + M_4u_{02}\Lambda_{22} = 0,\\ &M_2u_{02}\Lambda_{11} + M_1u_{02}\Lambda_{21} + M_4u_{02}\Lambda_{12} + \psi_{44}\Lambda_{22} = 0,\end{aligned} \tag{17}$$

where

$$\begin{aligned}\psi_{11} &= r_0 + M_1u_{01} - 2\rho\rho_0 - \rho_0^2 - 2\sigma\sigma_0 - \sigma_0^2,\\ \psi_{22} &= -r_0 + M_1u_{01} + 2\rho\rho_0 - \rho_0^2 + 2\sigma\sigma_0 - \sigma_0^2,\\ \psi_{33} &= r_0 + M_3u_{02} - 2\rho\rho_0 - \rho_0^2 - 2\sigma\sigma_0 - \sigma_0^2,\\ \psi_{44} &= -r_0 + M_3u_{02} + 2\rho\rho_0 - \rho_0^2 + 2\sigma\sigma_0 - \sigma_0^2.\end{aligned} \tag{18}$$

Equation (17) has nonzero solutions if and only if the determinant

$$\begin{vmatrix} \psi_{11} & M_2u_{01} & M_3u_{01} & M_4u_{01}\\ M_2u_{01} & \psi_{22} & M_4u_{01} & M_3u_{01}\\ M_1u_{02} & M_2u_{02} & \psi_{33} & M_4u_{02}\\ M_2u_{02} & M_1u_{02} & M_4u_{02} & \psi_{44}\end{vmatrix} = 0. \tag{19}$$

Substituting Eq. (18) into Eq. (19), we obtain the following dispersion relation:

$$r_0 = 2\rho\rho_0 + 2\sigma\sigma_0 \pm (\rho_0^2 + \sigma_0^2) \ \text{ or } \ r_0 = 2\rho\rho_0 + 2\sigma\sigma_0 \pm \sqrt{\Delta},$$

where $\Delta = (\rho_0^2 + \sigma_0^2)(\rho_0^2 + \sigma_0^2 - 4au_{01}^2 - 4bu_{01}u_{02} - 4\bar{b}u_{01}u_{02} - 4cu_{02}^2)$. If $\Delta \geq 0$, r_0 is real, and it follows that the steady state is stable against small perturbations. Otherwise, when $\Delta < 0$, r_0 is complex, and the steady state is unstable.

In the following, we consider the stability of the one periodic lump solution of Eq. (1) with the aid of the split-step Fourier method based on solution (5). Here, the exact solutions with 1% white noise added as initial conditions are inserted into Eq. (1) to test their stability against perturbations via direct numerical simulations. Figure 5 exhibits the numerical evolution of one periodic lump. From Fig. 5(a), the numerical solution for $t = 0.1$ shows no visible instability except for slight oscillations, and the white noise only slightly affects the background of the periodic lump. Comparing Fig. 5(b) with Fig. 5(a), the one periodic lump gradually becomes unstable as t increases, while other parameters remain unchanged. The periodic oscillation in the background begins to affect the periodic lump. When $t = 2$, the periodic lump cannot sustain its original shape; it becomes distorted, breaks up, and finally decays into noise, as shown in Fig. 5(c). The periodic lump (5) displays unstable evolution.

2.2. Double periodic lump solutions

The double periodic lump solutions can be expressed as

$$u_j = \frac{\Theta_4 \mathrm{e}^{\delta_1} n_j + \Theta_5 \mathrm{e}^{\delta_2} n_j + \Theta_1 n_j \alpha_1 + \Theta_2 n_j \alpha_2 + \delta_1 m_j \gamma_0 \left(1 + \Theta_{ij} A_{ij} + \Theta_6 \mathrm{e}^{\kappa_1}\right)}{1 + \Theta_{ij}\mu_{ij} + \Theta_6 \mathrm{e}^{\kappa_2}}, \tag{20}$$

where

$$\begin{aligned} &\Theta_1 = \cosh\theta_1 + \sinh\theta_1, \quad \Theta_2 = \cosh\theta_2 + \sinh\theta_2, \quad \Theta_{ij} = \cosh\theta_{ij} + \sinh\theta_{ij} \\ &\Theta_4 = \cosh\theta_4 + \sinh\theta_4, \quad \Theta_5 = \cosh\theta_5 + \sinh\theta_5, \quad \Theta_6 = \cosh\theta_6 + \sinh\theta_6, \end{aligned} \tag{21}$$

in which $i, j = 1, 2$, $\theta_4 = \theta_{11} + \theta_2$, $\theta_5 = \theta_{22} + \theta_1$, $\theta_6 = \theta_{11} + \theta_{22}$ and

$$\theta_2 = k_{12}x + k_{22}y + \mathrm{i}(-\lambda + k_{12}^2 + k_{22}^2)t + \xi_2, \quad \theta_{ij} = \left(k_{1i} + \bar{k}_{1j}\right)x + \left(k_{2i} + k_{2j}\right)y + \mathrm{i}\left(k_{1i}^2 + k_{2i}^2 - \bar{k}_{1j}^2 - \bar{k}_{2j}^2\right)t + \xi_i + \bar{\xi}_j. \tag{22}$$

The other parameters are given as follows:

$$\begin{aligned} &A_{11} = \frac{\mu_{11}\left[(k_{10} + \mathrm{i}k_{11})c_{11} + (k_{20} + \mathrm{i}k_{21})c_{22}\right]}{\left(k_{10} - \mathrm{i}\bar{k}_{11}\right)c_{11} + \left(k_{20} - \mathrm{i}\bar{k}_{21}\right)c_{22}}, \quad A_{12} = \frac{\mu_{12}\left[(k_{10} + \mathrm{i}k_{11})c_{14} + (k_{20} + \mathrm{i}k_{21})c_{25}\right]}{\left(k_{10} - \mathrm{i}\bar{k}_{12}\right)c_{14} + \left(k_{20} - \mathrm{i}\bar{k}_{22}\right)c_{25}}, \\ &A_{21} = \frac{\mu_{21}\left[(k_{10} + \mathrm{i}k_{12})\bar{c}_{14} + (k_{20} + \mathrm{i}k_{22})\bar{c}_{25}\right]}{\left(k_{10} - \mathrm{i}\bar{k}_{11}\right)\bar{c}_{14} + \left(k_{20} - \mathrm{i}\bar{k}_{21}\right)\bar{c}_{25}}, \quad A_{22} = \frac{\mu_{22}\left[(k_{10} + \mathrm{i}k_{12})c_{44} + (k_{20} + \mathrm{i}k_{22})c_{55}\right]}{\left(k_{10} - \mathrm{i}\bar{k}_{12}\right)c_{44} + \left(k_{20} - \mathrm{i}\bar{k}_{22}\right)c_{55}}, \end{aligned} \tag{23}$$

$$\mathrm{e}^{\delta_1} = \frac{\alpha_1\mu_{21}d_{12}\bar{c}_{14} + d_{22}\bar{c}_{25} - \alpha_2\mu_{11}d_{12}c_{11} + d_{22}c_{22}}{c_{11}\bar{c}_{14} + c_{22}\bar{c}_{25}}, \quad \mathrm{e}^{\delta_2} = \frac{\alpha_1\mu_{22}d_{12}c_{44} + d_{22}c_{55} - \alpha_2\mu_{12}d_{12}c_{14} + d_{22}c_{25}}{c_{14}c_{44} + c_{25}c_{55}}, \tag{24}$$

$$\begin{aligned} &\mathrm{e}^{\kappa_2} = \frac{\mathrm{e}^{\delta_2}\mu_{11}\left(\bar{d}_{12}c_{44} + \bar{d}_{22}c_{55}\right) - \mathrm{e}^{\delta_1}\mu_{12}\left(\bar{c}_{14}\bar{d}_{12} + \bar{c}_{25}\bar{d}_{22}\right)}{\alpha_1\left(\bar{c}_{14}c_{44} + \bar{c}_{25}c_{55}\right)}, \\ &\mathrm{e}^{\kappa_1} = \mathrm{e}^{\kappa_2}\frac{[(\mathrm{i}k_{12} + k_{10})\bar{c}_{14} + (\mathrm{i}k_{22} + k_{20})\bar{c}_{25}][(\mathrm{i}k_{11} + k_{10})c_{14} + (\mathrm{i}k_{21} + k_{20})c_{25}]}{[(k_{10} - \mathrm{i}\bar{k}_{11})\bar{c}_{14} + (k_{20} - \mathrm{i}\bar{k}_{21})\bar{c}_{25}][(k_{10} - \mathrm{i}\bar{k}_{12})c_{14} + (k_{20} - \mathrm{i}\bar{k}_{22})c_{25}]}. \end{aligned} \tag{25}$$

In above expressions the μ_{ij} satisfy the constraint conditions

$$\begin{aligned} &\mu_{11} = \frac{|\alpha_1|^2 l}{c_{11}^2 + c_{22}^2}\left\{1 + \frac{\lambda(c_{11}^2 + c_{22}^2)}{2\mathrm{i}\left[(k_{11} - \mathrm{i}k_{10})c_{11} + (k_{21} - \mathrm{i}k_{20})c_{22}\right]\left[(k_{10} - \mathrm{i}\bar{k}_{11})c_{11} + (k_{20} - \mathrm{i}\bar{k}_{21})c_{22}\right]}\right\}^{-1}, \\ &\mu_{12} = \frac{\alpha_1\bar{\alpha}_2 l}{c_{14}^2 + c_{25}^2}\left\{1 + \frac{\lambda(c_{14}^2 + c_{25}^2)}{2\mathrm{i}[(k_{11} - \mathrm{i}k_{10})c_{14} + (k_{21} - \mathrm{i}k_{20})c_{25}][(k_{10} - \mathrm{i}\bar{k}_{12})c_{14} + (k_{20} - \mathrm{i}\bar{k}_{22})c_{25}]}\right\}^{-1}, \\ &\mu_{21} = \frac{\alpha_2\bar{\alpha}_1 l}{\bar{c}_{14}^2 + \bar{c}_{25}^2}\left\{1 + \frac{\lambda(\bar{c}_{14}^2 + \bar{c}_{25}^2)}{2\mathrm{i}[(k_{12} - \mathrm{i}k_{10})\bar{c}_{14} + (k_{22} - \mathrm{i}k_{20})\bar{c}_{25}][(k_{10} - \mathrm{i}\bar{k}_{11})\bar{c}_{14} + (k_{20} - \mathrm{i}\bar{k}_{2})\bar{c}_{25}]}\right\}^{-1}, \\ &\mu_{22} = \frac{|\alpha_2|^2 l}{c_{44}^2 + c_{55}^2}\left\{1 + \frac{\lambda(c_{44}^2 + c_{55}^2)}{2\mathrm{i}\left[(k_{12} - \mathrm{i}k_{10})c_{44} + (k_{22} - \mathrm{i}k_{20})c_{55}\right]\left[(k_{10} - \mathrm{i}\bar{k}_{12})c_{44} + (k_{20} - \mathrm{i}\bar{k}_{22})c_{55}\right]}\right\}^{-1}, \end{aligned} \tag{26}$$

and $c_{14} = k_{11} + \bar{k}_{12}$, $c_{25} = k_{21} + \bar{k}_{22}$, $c_{44} = k_{12} + \bar{k}_{12}$, $c_{55} = k_{22} + \bar{k}_{22}$, $d_{12} = k_{11} - k_{12}$, $d_{22} = k_{21} - k_{22}$. The other parameters α_j, k_j, ξ_j $(j = 1, 2)$ and γ_0 are arbitrary complex constants. Moreover, μ_{11} and μ_{22} are real constants while μ_{12} and μ_{21} are complex constants.

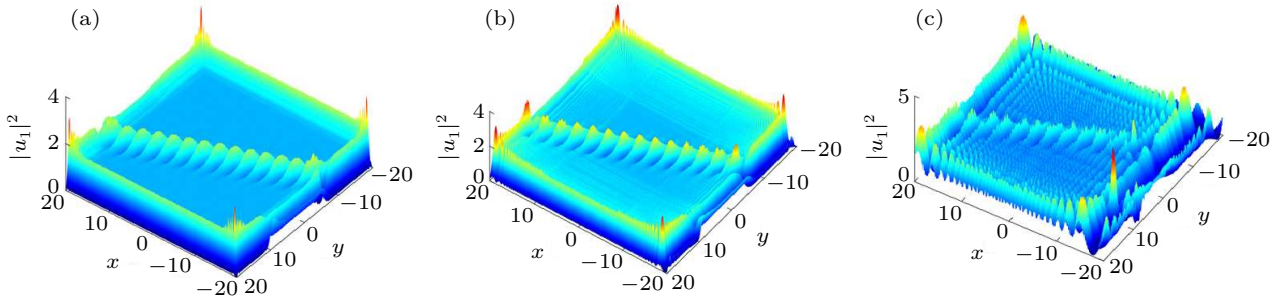


Fig. 5. Evolutions of one periodic lump given by Eq. (5) under an initial white noise perturbation of 1% from $t = 0$ to (a) $t = 0.1$, (b) $t = 0.4$, and (c) $t = 2$. The parameters are the same as those used in Fig. 1(b).

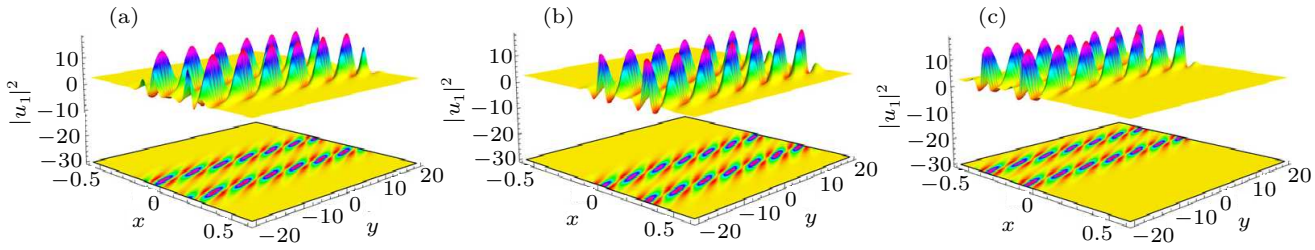


Fig. 6. Double periodic lumps propagating along the x-axis with $\xi_1 = 0$, $\xi_2 = 0$, $k_{10} = 50$, $k_{20} = 1$, $a = 200$, $b = 20$, $c = 10$, $k_{21} = 0.01\mathrm{i}$, $k_{22} = -0.01\mathrm{i}$, $m_2 = 1$, $n_1 = 10$, $n_2 = 1$, $\alpha_1 = 1$, $\alpha_2 = 10$, $\gamma_0 = 15.9$, $k_{11} = 32 + 0.01\mathrm{i}$, $k_{12} = 30 + 0.01\mathrm{i}$. (a) $t = 0$; (b) $t = 5$; (c) $k_{11} = 32 - 0.03\mathrm{i}$, $k_{12} = 30 - 0.03\mathrm{i}$, $t = 5$.

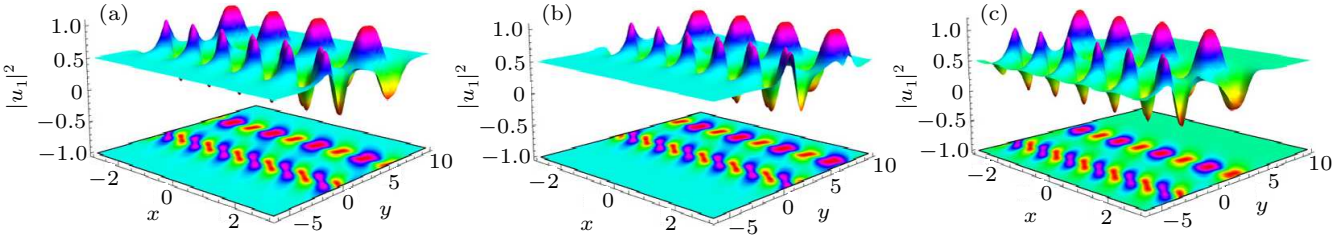


Fig. 7. Double periodic lumps propagating along the y-axis with $\xi_1 = 0$, $\xi_2 = 0$, $k_{10} = 5$, $k_{20} = 1$, $a = 0.1$, $b = 2$, $c = 1$, $k_{11} = 0.91\mathrm{i}$, $k_{12} = -0.91\mathrm{i}$, $m_2 = 1$, $n_1 = 1$, $n_2 = 1$, $\alpha_1 = 0.001$, $\alpha_2 = 1$, $\gamma_0 = 0.5$, $k_{21} = 1.5 + 0.05\mathrm{i}$, $k_{22} = 1.5 + 0.05\mathrm{i}$. (a) $t = 0$; (b) $t = 15$; (c) $k_{21} = 1.5 - 0.1\mathrm{i}$, $k_{22} = 1.5 - 0.1\mathrm{i}$, $t = 15$.

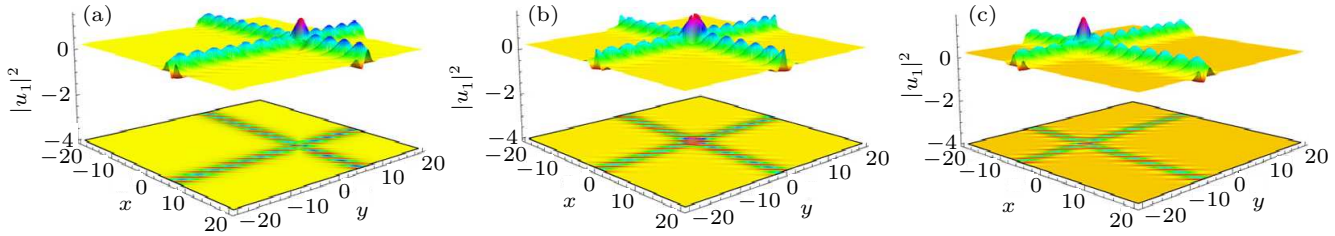


Fig. 8. Interaction of double periodic lumps with $\xi_1 = 0$, $\xi_2 = 0$, $k_{10} = 1$, $k_{20} = 1$, $a = 1$, $b = 1$, $c = 1$, $k_{11} = 3\mathrm{i}$, $k_{21} = 1 - \mathrm{i}$, $k_{12} = 1 - \mathrm{i}$, $k_{22} = 3\mathrm{i}$, $m_2 = 1$, $n_1 = 1$, $n_2 = 1$, $\alpha_1 = 1$, $\alpha_2 = 1$, $\gamma_0 = 0.5$. (a) $t = -3$; (b) $t = 0$; (c) $t = 3$.

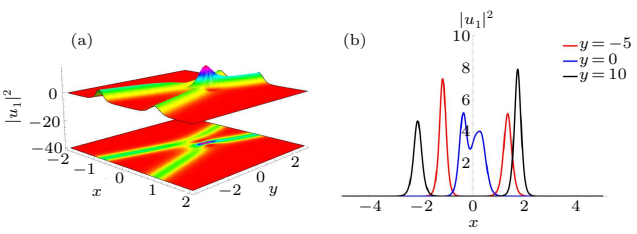


Fig. 9. Bright two-soliton solutions for Eq. (1) with $\xi_1 = 0$, $\xi_2 = 0$, $a = 1$, $b = 1$, $c = 1$, $k_{10} = 1$, $k_{20} = 1$, $k_{11} = -6 + \mathrm{i}$, $k_{21} = 1$, $k_{12} = 5 + 5\mathrm{i}$, $k_{22} = 1$, $m_2 = 1$, $n_1 = 0.8$, $n_2 = 1$, $\alpha_1 = 1$, $\alpha_2 = 1$, $\gamma_0 = 0$, $t = 0$. Panel (b) shows the cross-sectional view of (a).

In order to represent the velocities of periodic lump waves in a uniform and clear manner, we use the orthogonal decomposition method to represent the velocities and directions of wave motion, i.e., the velocities are shown on the x-axis and y-axis, respectively. The velocities of double periodic lump waves can be given in component form as

$$V_1 = \left(\frac{2\Upsilon_1 k_{11R}}{k_{11R}^2 + k_{21R}^2}, \frac{2\Upsilon_1 k_{21R}}{k_{11R}^2 + k_{21R}^2} \right),$$

$$V_2 = \left(\frac{2\Upsilon_2 k_{12R}}{k_{12R}^2 + k_{22R}^2}, \frac{2\Upsilon_2 k_{22R}}{k_{12R}^2 + k_{22R}^2} \right),$$

where $\Upsilon_1 = k_{21I}k_{21R} + k_{11I}k_{11R}$ and $\Upsilon_2 = k_{22I}k_{22R} + k_{12I}k_{12R}$. In Fig. 6, the periodic lumps move along the x-axis and their velocities are $(2k_{11I}, 0)$ and $(2k_{12I}, 0)$ respectively. The parameters k_{11I} and k_{12I} are both positive in Figs. 6(a) and 6(b), so the double periodic lumps propagate in the direction of $x > 0$. When we change the sign and magnitude of k_{11I} and k_{12I} as shown in Fig. 6(c), we see that the double periodic lumps propagate in the opposite direction to Fig. 6(a), and their speed increases as time t increases. Obviously, the magnitude of the velocity is adjusted by $|k_{11I}|$ and $|k_{12I}|$. Figure 7 illustrates that they move along the y-axis without any interaction, and the motion velocities of the periodic lumps are $(0, 2k_{21I})$ and $(0, 2k_{22I})$. Figure 8 shows the interaction phenomenon of the double periodic lumps as follows: one moves along the x-axis, and the other moves along the y-axis. As shown in Figs. 8(a)–8(c), the velocities of the two periodic lumps are $(-2, 0)$ and $(0, -2)$. When t varies from -3 to 3, they propagate in the direction of $x < 0$ and $y < 0$. Similarly, when we reverse the sign of the velocities, the double periodic lumps propagate in the direction of $x > 0$ and $y > 0$. We can also obtain the intersecting bright two-soliton solutions as shown in Figs. 9(a)

and 9(b) respectively. By observing Fig. 9, we can see that the intensity of the two bright solitons changes before and after collision, indicating that the above collision is inelastic.

3. Lump and mixed solutions of the coupled NLS equations

3.1. One lump on a periodic wave background

In order to obtain a one-lump solution of Eq. (1), we set $\xi_1 = \mathrm{i}\pi$ in Eq. (5) and apply the long-wave limit method. The expression for u_1 can be simplified as follows:

$$u_1 = \frac{-2-1.4x+(1+\mathrm{i})y-0.4\,\mathrm{e}^{\mathrm{i}(5.5x+y)}p_{10}}{1.86978-1.78503\mathrm{i}+q_{10}}, \tag{27}$$

where

$$\begin{aligned} p_{10} &= 2.02306-0.852342\mathrm{i} \\ &\quad +(1.43229-1.19328\mathrm{i})\,[x+(1+\mathrm{i})y], \\ q_{10} &= (1.21769-2.49905\mathrm{i})\,[x+(1+\mathrm{i})y], \end{aligned} \tag{28}$$

for the parameters $a=1$, $b=0.1$, $c=1$, $k_{11}=0.7$, $k_{21}=0.7+0.7\mathrm{i}$, $k_{10}=5.5$, $k_{20}=1$, $m_2=n_1=n_2=1$, $\alpha_1=0.1$, and $\gamma_0=0.4$.

Figure 10 shows the evolution of the lump on the periodic wave background. A single lump on a plane wave background is shown in Fig. 11(a) when $\gamma_0=0$. Reducing the value of k_{10} decreases the period of the background wave, as shown in Fig. 11(b). Compared with Fig. 11(b), both the peak of the lump solution and the period of the background wave increase, and the propagation direction of the background wave also changes when $k_{20}=16$, as shown in Fig. 11(c).

Thus, the background period of the lump solution is determined by the parameters γ_0, k_{10}, and k_{20}.

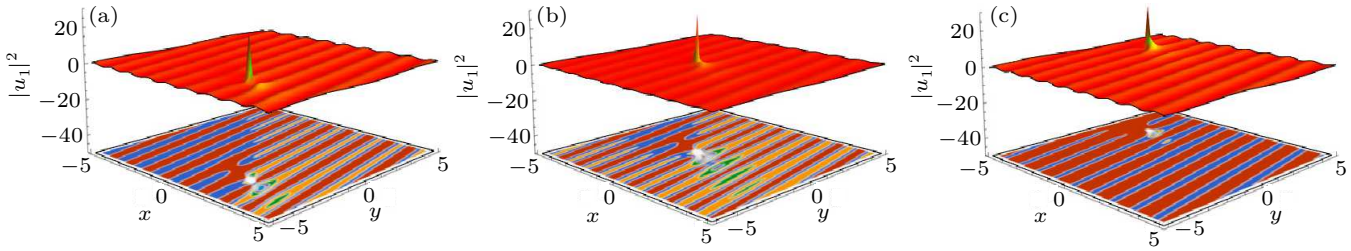


Fig. 10. The motion of one lump on the periodic wave background for Eq. (1) via solution (27) at (a) $t=-3$, (b) $t=0$, and (c) $t=3$.

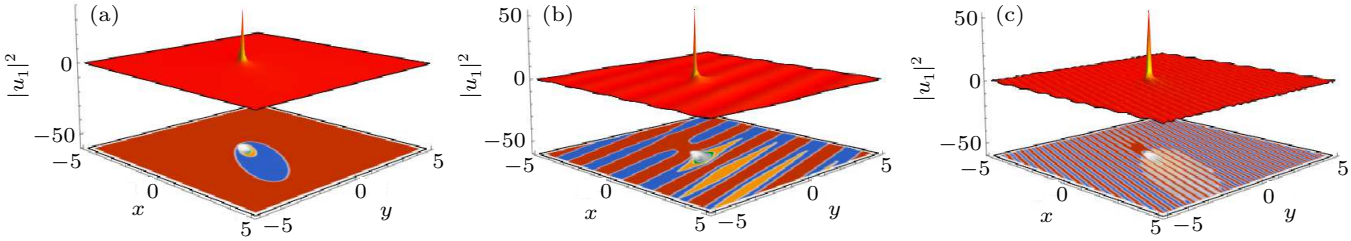


Fig. 11. One lump solution of Eq. (1) with (a) $\gamma_0=0$, $k_{10}=5.5$, $k_{20}=1$; (b) $\gamma_0=0.6$, $k_{10}=3.5$, $k_{20}=1$; and (c) $\gamma_0=6$, $k_{10}=5.5$, $k_{20}=16$.

3.2. Two lumps on a periodic wave background

To obtain the two-lump solutions of Eq. (1), we set $\xi_j = \mathrm{i}\pi$ $(j=1,2)$, $\bar{k}_{22}=k_{21}$, and $\bar{k}_{12}=k_{11}$ in Eq. (20) and apply the long-wave limit method under the conditions $k_{11}\to 0$ and $k_{12}\to 0$. The expression for u_1 can then be simplified as

$$u_1 = \frac{p_{11}+\mathrm{e}^{12\mathrm{i}(x+y)}p_{12}}{q_{11}}, \tag{29}$$

where

$$\begin{aligned} p_{11} &= 0.000693247+0.0014429\mathrm{i}\ +(0.00441233+0.0083018\mathrm{i})x^2+\Big[(0.0029939+0.00591298\mathrm{i}) \\ &\quad -(0.00777895-0.0254283\mathrm{i})y\Big]x-(0.00291908-0.00890689\mathrm{i})y-(0.0166036-0.00882465\mathrm{i})y^2, \\ p_{12} &= -0.0389985+0.011291\mathrm{i}-(0.427214-0.151948\mathrm{i})x^2+\Big[-0.293984+0.0974871\mathrm{i} \\ &\quad -(1.15832+0.550533\mathrm{i})y\Big]x-(0.391471+0.196497\mathrm{i})y-(0.303895+0.854428\mathrm{i})y^2, \\ q_{11} &= 0.0868191+0.00633578\mathrm{i}+(0.675836+0.0171871\mathrm{i})x+x^2+(0.658649+0.693023\mathrm{i})y+(2+2\mathrm{i})xy+2\mathrm{i}y^2, \end{aligned}$$

for the parameters $a = 7$, $b = 1+2\mathrm{i}$, $c = 1.5$, $k_{11} = 3$, $k_{21} = 3+3\mathrm{i}$, $k_{12} = 1$, $k_{22} = 1+\mathrm{i}$, $k_{10} = k_{20} = 12$, $m_2 = 1$, $n_1 = 0.1$, $n_2 = 1$, $\alpha_1 = \alpha_2 = 3.5$, and $\gamma_0 = 1$.

Figure 12 illustrates the evolution of the two lumps on a periodic wave background. The two lumps on a plane wave background are shown in Fig. 13 for the case $k_{10} = k_{20} = 1$.

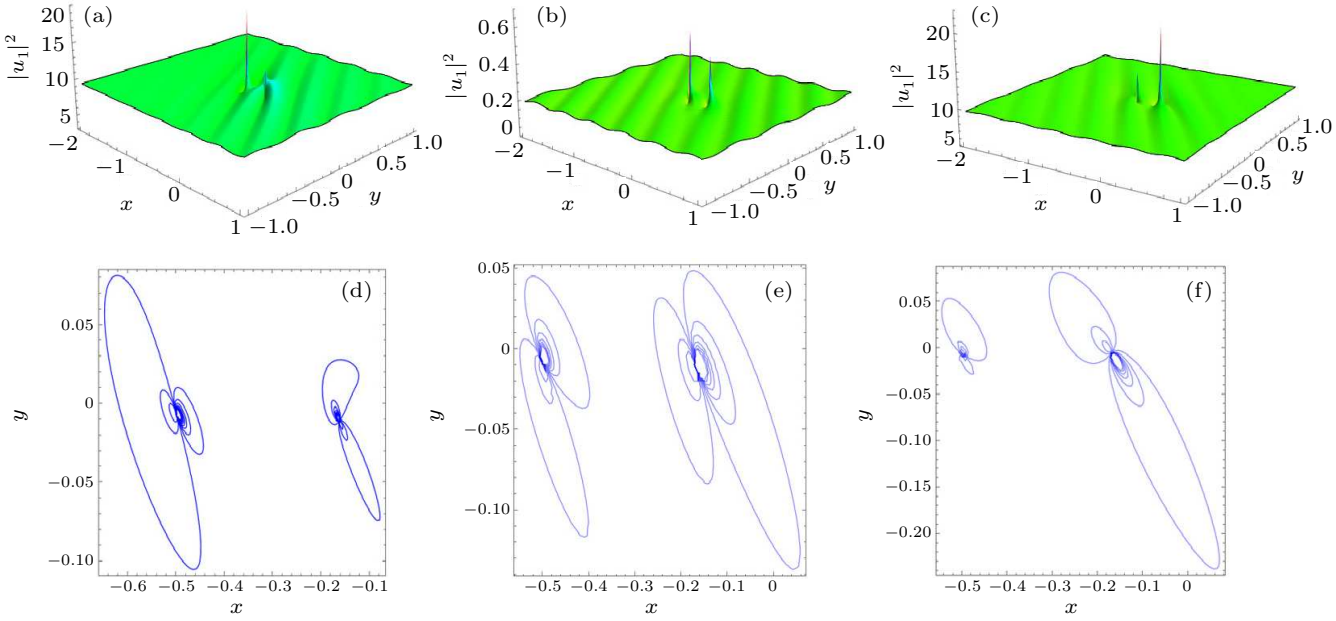


Fig. 12. Double lump solutions on the periodic wave background with (a) $t = -2$; (b) $t = 0$; (c) $t = 2$; (d)–(f) contour profiles.

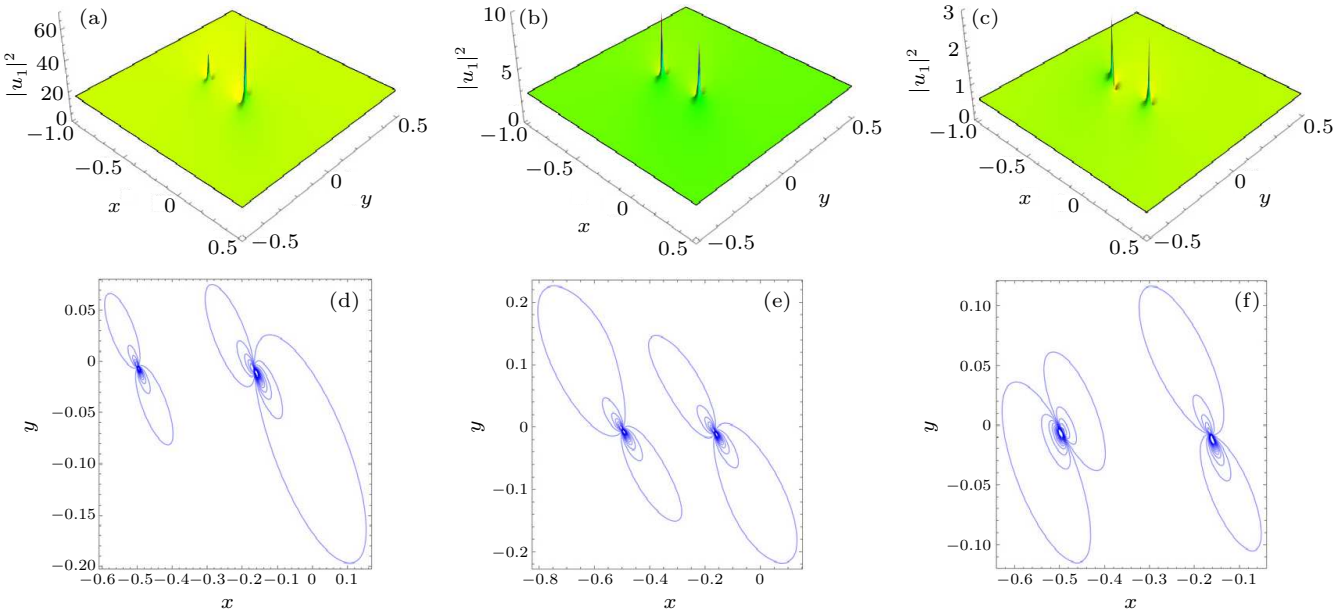


Fig. 13. Double lump solutions on the plane wave background with (a) $t = -0.5$; (b) $t = 0$; (c) $t = 0.5$; (d)–(f) contour profiles.

3.3. Multi-lumps and mixed solutions

To obtain the mixed solutions of one lump and double periodic lump solutions of Eq. (1), we apply the long-wave limit method under the condition $k_{11} \to 0$. The expression for u_1 can be simplified as

$$u_1 = \frac{0.359375\,\mathrm{e}^{\mathrm{i}(x+2y)} p_{21} + 1.5 p_{22}}{q_{21}},$$

where

$$\begin{aligned}
p_{21} &= 1.8426 + 1.40549\mathrm{i} - (3456.58 - 24235.9\mathrm{i})\,\mathrm{e}^{2x+0.1y} - \Big[(2207.59 + 402.694\mathrm{i}) + (12275.4 + 2706.15\mathrm{i})(x + Y_2)\Big]\,\mathrm{e}^{4x+0.2y} \\
&\quad + (2.8 + 0.1\mathrm{i})(x + Y_2)\Big[1.6852 + 2.81099\mathrm{i} - (3456.58 - 24235.9\mathrm{i})\,\mathrm{e}^{2x+0.1y}\Big], \\
p_{22} &= 0.1 - (4941.19 - 4493.25\mathrm{i})\,\mathrm{e}^{2x+0.1y} + (0.826373 + 0.227989\mathrm{i})\,\mathrm{e}^{4x+0.2y} + (2.8 + 0.1\mathrm{i})
\end{aligned}$$

$$\times\Big[0.1(x+Y_2)+(0.826373+0.227989\mathrm{i})(x+Y_2)\,\mathrm{e}^{4x+0.2y}-(5041.19-4493.25\mathrm{i})(2x+(2.6+1.8\mathrm{i})y)\,\mathrm{e}^{2x+0.1y}\Big],$$

$$q_{21} = 1.30646-0.297752\mathrm{i}-(18023.2+991.589\mathrm{i})\,\mathrm{e}^{2x+0.1y}+\Big[(479.185-338.361\mathrm{i})+(2739.53-1799.4\mathrm{i})(x+Y_2)\Big]\,\mathrm{e}^{4x+0.2y}$$
$$+(2.8+0.1\mathrm{i})(x+Y_2)\Big[(0.612928-0.595503\mathrm{i})-(18023.2+991.589\mathrm{i})\,\mathrm{e}^{2x+0.1y}\Big],$$

with $Y_2=(1.3+0.9\mathrm{i})y$, and the parameters chosen as $a=1$, $b=0.1$, $c=1$, $k_{11}=2.8+0.1\mathrm{i}$, $k_{21}=2.55+2.45\mathrm{i}$, $k_{12}=2$, $k_{22}=0.1$, $k_{10}=2$, $k_{20}=2$, $m_2=1$, $n_1=1.5$, $n_2=1$, $\alpha_1=0.1$, $\alpha_2=100$, $\gamma_0=0.5$, with other parameters as given in Fig. 12.

The resulting mixed solutions of one lump and double periodic lumps are shown in Fig. 14(a). When $k_{22}=1.9$, a one-lump solution appears between a periodic lump and a dark soliton on the periodic wave background, as illustrated in Fig. 14(b). Further increasing k_{22} leads to two anti-dark soliton structures on either side of the lump and an increase in the period of the background wave, as shown in Fig. 14(c). By increasing the parameter a as in Fig. 14(d), the peaks of the periodic lump solutions increase and they reside on a plane wave background, while the one lump approaches the periodic lump on the right. Changing k_{10} allows the one lump and multi-peak solitons to merge into a single structure, as seen in Fig. 14(e). Figure 14(f) shows the integration of one lump and a single periodic lump for the parameters $a=2$, $b=0.1$, $c=1$, $k_{11}=3$, $k_{21}=4.5+2.7\mathrm{i}$, $k_{12}=3$, $k_{22}=15$, $k_{10}=k_{20}=m_2=1$, $n_1=1.5$, $n_2=0$, $\alpha_1=0.03$, $\alpha_2=100$, and $\gamma_0=1.5$.

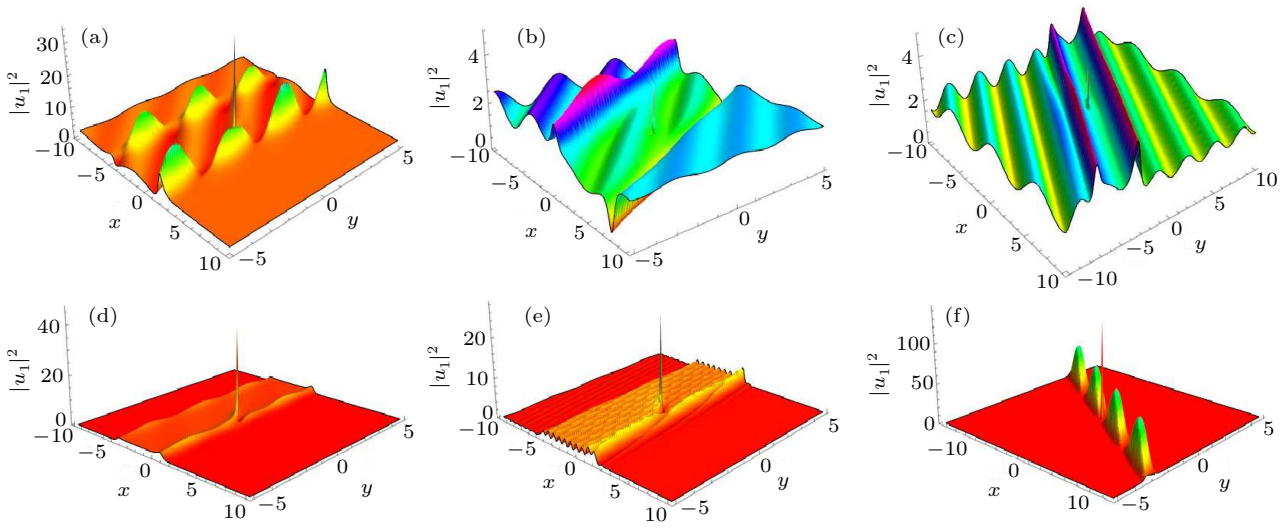


Fig. 14. Mixed solutions for Eq. (1) with (a) $k_{22}=0.1$; (b) $k_{22}=1.9$; (c) $k_{22}=5.85$; (d) $a=10$; (e) $k_{10}=9$; (f) $a=2$, $b=0.1$, $c=1$, $k_{11}=3$, $k_{21}=4.5+2.7\mathrm{i}$, $k_{12}=3$, $k_{22}=15$, $k_{10}=k_{20}=m_2=1$, $n_1=1.5$, $n_2=0$, $\alpha_1=0.03$, $\alpha_2=100$, $\gamma_0=1.5$.

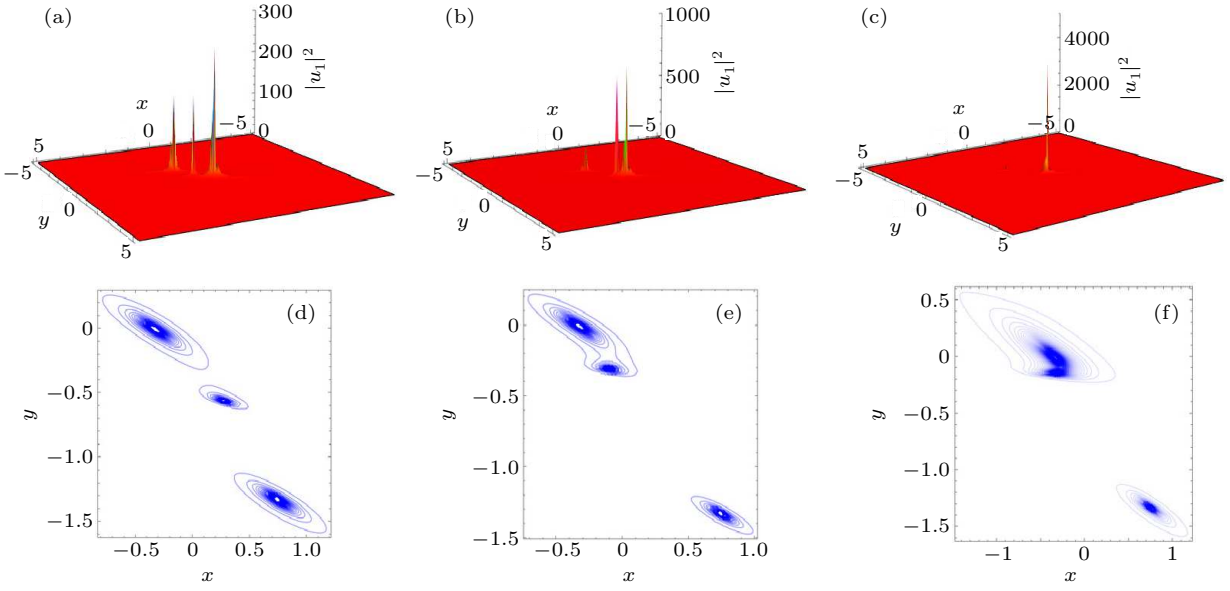


Fig. 15. Three-lump solutions with (a) $k_{22}=12$; (b) $k_{22}=15$; (c) $k_{22}=21$; (d)–(f) contour profiles.

At the same time, three-lump solutions can be obtained as

$$u_1 = \frac{3.87446 - 0.637224\mathrm{i} + p_{31}}{-90.965 + 21.7213\mathrm{i} + q_{31}}, \tag{30}$$

where

$$\begin{aligned}
p_{31} =\ & (11.6234 - 1.91167\mathrm{i})x + (19.1556 + 7.59352\mathrm{i})y \\
& + \mathrm{e}^{3(x+4y)}\Big[(12824 - 2215.84\mathrm{i}) \\
& - (545.298 + 550.536\mathrm{i})x \\
& - (322.465 + 1316.57\mathrm{i})y\Big] \\
& + \mathrm{e}^{6(x+4y)}\Big[-0.0147702 - 0.0106919\mathrm{i} \\
& - (0.0443107 + 0.0320756\mathrm{i})x \\
& - (0.037598 + 0.0879931\mathrm{i})y\Big], \\
q_{31} =\ & -(29.1959 - 45.3648\mathrm{i})x - (84.6221 - 41.7709\mathrm{i})y \\
& + \mathrm{e}^{3(x+4y)}\Big[-2704.87 + 11460.1\mathrm{i} \\
& - (8114.6 - 34380.3\mathrm{i})x \\
& - (43114.2 - 44267.4\mathrm{i})y\Big] \\
& + \mathrm{e}^{6(x+4y)}\Big[-1.73258 + 0.312365\mathrm{i} \\
& + x + (1.5 + 0.9\mathrm{i})y\Big].
\end{aligned}$$

These are illustrated in Fig. 15(a) for the parameters $a = 2$, $b = 0.1$, $c = 1$, $k_{11} = 3$, $k_{21} = 4.5 + 2.7\mathrm{i}$, $k_{12} = 3$, $k_{22} = 12$, $k_{10} = 0$, $k_{20} = 1$, $m_2 = 0$, $n_1 = 1.5$, $n_2 = 0$, $\alpha_1 = 0.03$, $\alpha_2 = 100$, $\gamma_0 = 1$, and $t = 0$. By increasing k_{22}, two of the lumps merge into a single lump, forming two-lump structures as shown in Figs. 15(b) and 15(c). In this way, multiple mixed solutions can be obtained from the double periodic lumps by appropriately adjusting the parameters, as illustrated in Figs. 14 and 15.

4. Conclusion

In this paper, we systematically obtained various types of solutions for the generalized coupled NLS system. A key contribution is the derivation of periodic lump solutions for Eq. (1), with single and double periodic lump structures on plane wave backgrounds illustrated in Figs. 1 and 6–8. Parameter analysis revealed that k_{11} modulates the periodicity of the periodic lump solutions, as shown in Fig. 2. Bright-dark W-shaped, multi-peak, and bright soliton solutions were obtained by assigning specific parameter values, and their spatiotemporal dynamics were visualized in Figs. 3 and 4. Critical dependencies on parameters were identified, with k_{j0}, k_{j1}, and k_{j2} being key factors determining the number of soliton peaks. The stability of the numerical solutions was also investigated, with results shown in Fig. 5. Two-soliton solutions were derived as well, revealing collision behaviors of bright solitons (Fig. 9).

By applying the long-wave limit method, these solutions yielded corresponding lump solutions propagating on periodic and plane wave backgrounds, as depicted in Figs. 10–13. Furthermore, mixed solutions combining periodic lumps, single lumps, and solitons were constructed and analyzed in Figs. 14 and 15, highlighting their potential for exploring nonlinear interactions. These results provide a versatile framework applicable to nonlinear models across various disciplines, and future work will extend this methodology to higher-dimensional nonlinear evolution equations.

The solitons and their interactions obtained in this study are closely related to bound soliton states recently observed in fiber laser experiments,[47–49] suggesting potential experimental realization in nonlinear optical systems. In particular, the generation of vector solitons with compound pulsation periods using carbon black/graphene oxide saturable absorbers[47] demonstrates that complex periodic and multi-peak soliton dynamics can be reliably generated and maintained in laser cavities. Similarly, deep learning-based modeling of vector-soliton pulsations in Ref. [48] shows that intricate soliton interactions can be accurately predicted and experimentally validated, underscoring the relevance of these solutions to physical systems. Moreover, polarization-controlled switching dynamics between soliton molecules and noise-like pulses highlight the critical roles of nonlinearity, dispersion, and cavity feedback in stabilizing multi-soliton states.[49] The soliton interaction behaviors discussed in this paper correspond to these experimental observations, particularly under the influence of cross-phase modulation and higher-order effects. We anticipate that the soliton and lump solutions presented here could be experimentally realized in fiber lasers with appropriate saturable absorbers, polarization settings, and dispersion profiles. This consistency between our analytical results and recent experimental advances points to potential applications in designing multi-functional fiber lasers and advanced information encoding systems.

Acknowledgment

This work was supported by the Applied Basic Research Program of Shanxi Province, China (Grant Nos. 202403021212253 and 202203021221217).

References

[1] Yang C Y, Liu W J, Zhou Q, *et al.* 2019 *Nonlinear Dyn.* **95** 369
[2] Agalarov A, Zhulego V and Gadzhimuradov T 2015 *Phys. Rev. E* **91** 042909
[3] Som B K, Gupta M R and Dasgupta B 1979 *Phys. Lett. A* **72** 111
[4] Ding C C, Zhou Q and Malomed B A 2025 *Phys. Rev. E* **111** 044203
[5] Zhong Y, Yang D F, Liu Y X, *et al.* 2025 *Chin. Phys. Lett.* **42** 080002
[6] Zhong Y, Triki H and Zhou Q 2024 *Chin. Phys. Lett.* **41** 070501
[7] Kanna T and Lakshmanan M 2001 *Phys. Rev. Lett.* **86** 5043
[8] Wong P, Liu W J, Huang L G, *et al.* 2015 *Phys. Rev. E* **91** 033201
[9] Yang W, Cheng X P, Jin G M, *et al.* 2023 *Chin. Phys. B* **32** 120202
[10] Lan H, Chen F, Komarov A, *et al.* 2024 *Phys. Rev. A* **110** 053505

[11] Pu H and Bigelow N P 2003 *Phys. Rev. Lett.* **90** 140401
[12] Ajmani M, Singh P and Kaur P 2019 *Wireless Pers. Commun.* **107** 959
[13] Wang M, Xu T, He G L, *et al.* 2023 *Chin. Phys. B* **32** 050503
[14] Manakov S V, Zakharov V E, Bordag L A, *et al.* 1977 *Phys. Lett. A* **63** 205
[15] Chen S J, Lv X and Yin Y 2023 *Commun. Theor. Phys.* **75** 055005
[16] An Y N and Guo R 2023 *Nonlinear Dyn.* **111** 18291
[17] Pan Y, Manafian J, Zeynalli S M, *et al.* 2022 *Qual. Theory Dyn. Syst.* **21** 127
[18] Ying L and Li M 2023 *Nonlinear Dyn.* **111** 15633
[19] Chen J and Pelinovsky D E 2021 *Phys. Rev. E* **103** 062206
[20] Ma Y L and Li B Q 2024 *Nonlinear Dyn.* **112** 2851
[21] Wu Z J and Tian S F 2023 *Comput. Simulat.* **210** 235
[22] Zhang X, Wang L, Liu C, *et al.* 2020 *Chaos* **30** 113107
[23] Yin Z Y and Tian S F 2021 *Physica D* **427** 133002
[24] Wen S, Manafian J, Sedighi S, *et al.* 2024 *Sci. Rep.* **14** 19568
[25] Shen S, Jin Y and Zhang J 2014 *Rep. Math. Phys.* **73** 255
[26] Alsufi N A, Fatima N, Noor A, *et al.* 2023 *Chaos Soliton Fract.* **170** 113410
[27] Zahran E H M and Bekir A 2022 *Int. J. Mod. Phys. B* **36** 2250166
[28] Pang F, Gegen H and Zhao X 2023 *Chin. Phys. B* **32** 050205
[29] Yang S X, Wang Y F and Jia R R 2023 *Phys. Scr.* **98** 125208
[30] Stepanyants Y D, Zakharov D V and Zakharov V E 2022 *Radiophys Quant. El.* **64** 665
[31] Li Y, Yao R, Xia Y, *et al.* 2021 *Commun. Nonlinear Sci. Numer. Simulat.* **100** 105843
[32] Yao R, Li Y and Lou S 2021 *Commun. Nonlinear Sci. Numer. Simulat.* **99** 105820
[33] Radha R, Vinayagam P S and Porsezian K 2016 *Commun. Nonlinear Sci. Numer. Simulat.* **37** 354
[34] Wang L, Luan Z, Zhou Q, *et al.* 2021 *Nonlinear Dyn.* **104** 2613
[35] Agalarov A, Zhulego V and Gadzhimuradov T 2015 *Phys. Rev. E* **91** 042909
[36] Singh S and Ray S S 2023 *Chaos Soliton Fract.* **175** 113947
[37] Rao J, Mihalache D, He J, *et al.* 2022 *Commun. Nonlinear Sci. Numer. Simulat.* **110** 106382
[38] Yulin A V and Zezyulin D A 2022 *Phys. Rev. E* **106** 044202
[39] Wang M, Tian B, Qu Q X, *et al.* 2021 *Mod. Phy.s Lett. B* **35** 2150020
[40] Ding C C, Zhu L W, Triki H, *et al.* 2024 *Physica D* **464** 134191
[41] Ismael H F 2023 *Results Phys.* **53** 106965
[42] Guan X, Liu W J, Zhou Q, *et al.* 2020 *Appl. Math. Comput.* **366** 124757
[43] Ma H C, Mao X and Deng A P 2023 *Chin. Phys. B* **32** 060201
[44] Guo F and Lin J 2020 *Mod. Phys. Lett. B* **34** 2050384
[45] Yin Y H, Chen S J and Lv X 2020 *Chin. Phys. B* **29** 120502
[46] Hu X R, Shen S F and Jin Y Y 2019 *Appl. Math. Lett.* **90** 99
[47] Ju Z T, Si Z Z, Yan X, *et al.* 2024 *Chin. Phys. Lett.* **41** 084203
[48] Si Z Z, Wang D L, Zhu B W, *et al.* 2024 *Laser Photonics Rev.* **18** 2400097
[49] Si Z Z, Ju Z T, Ren L F, *et al.* 2025 *Laser Photonics Rev.* **19** 2401019